Regnase-1 controls colon epithelial regeneration via regulation of mTOR and purine metabolism

Yasuharu Nagahama[a,b,c,1], Mayuko Shimoda[a,c,1], Guoliang Mao[a,c,1], Shailendra Kumar Singh[a], Yuuki Kozakai[a,c,d], Xin Sun[a,c], Daisuke Motooka[e], Shota Nakamura[e], Hiroki Tanaka[a], Takashi Satoh[a,c], Kazuhiko Maeda[a,c], and Shizuo Akira[a,c,2]

[a]Laboratory of Host Defense, The World Premier International Research Center Initiative (WPI) Immunology Frontier Research Center, Osaka University, 565-0871 Osaka, Japan; [b]Fujii Memorial Research Institute, Otsuka Pharmaceutical Company, Ltd., 520-0106 Shiga, Japan; [c]Laboratory of Host Defense, Research Institute for Microbial Diseases, Osaka University, 565-0871 Osaka, Japan; [d]Tokushima Research Institute, Otsuka Pharmaceutical Company, Ltd., 771-0192 Tokushima, Japan; and [e]Genome Information Research Center, Research Institute for Microbial Diseases, Osaka University, 565-0871 Osaka, Japan

Contributed by Shizuo Akira, September 4, 2018 (sent for review June 5, 2018; reviewed by Koji Hase and Markus Neurath)

Damage to intestinal epithelial cell (IEC) layers during intestinal inflammation is associated with inflammatory bowel disease. Here we show that the endoribonuclease Regnase-1 controls colon epithelial regeneration by regulating protein kinase mTOR (the mechanistic target of rapamycin kinase) and purine metabolism. During dextran sulfate sodium-induced intestinal epithelial injury and acute colitis, Regnase-1$^{\Delta IEC}$ mice, which lack Regnase-1 specifically in the intestinal epithelium, were resistant to body weight loss, maintained an intact intestinal barrier, and showed increased cell proliferation and decreased epithelial apoptosis. Chronic colitis and tumor progression were also attenuated in Regnase-1$^{\Delta IEC}$ mice. Regnase-1 predominantly regulates mTORC1 signaling. Metabolic analysis revealed that Regnase-1 participates in purine metabolism and energy metabolism during inflammation. Furthermore, increased expression of ectonucleotidases contributed to the resolution of acute inflammation in Regnase-1$^{\Delta IEC}$ mice. These findings provide evidence that Regnase-1 deficiency has beneficial effects on the prevention and/or blocking of intestinal inflammatory disorders.

RNA stability | inflammatory bowel disease | purine metabolism | mTOR | epithelial regeneration

Intestinal epithelial cells (IECs) cooperate to maintain homeostasis with the commensal microbiota in the intestinal tract (1). Inflammatory bowel disease (IBD) is a chronic inflammatory condition of the intestinal tract caused by disrupted IEC layers. IBD inducers, including poor diet and enteral nutritional factors, are risk factors for human colorectal cancer (CRC) (2). Experimental animal models for IBD provide valuable insight into the complex mechanisms of IBD (3).

The mechanistic target of rapamycin kinase (mTOR) is a conserved serine–threonine kinase in both yeast and mammals. mTOR signaling plays essential roles in health and disease by distinct mechanisms (4). In vivo studies using knockout mice have revealed varied physiological functions of mTOR signaling (5). mTORC1 is a signaling complex containing mTOR that acts as an important integrator of nutrient-sensing pathways to control cell growth and survival. A major role of mTORC1 is in amino acid sensing, but mTORC1 also stimulates nucleotide biosynthesis to control anabolic processes (6–8). This sensing mechanism coordinates reprogramming of energy metabolism to promote cell growth and proliferation. mTOR signaling is a key therapeutic drug target for several diseases, including CRC (9). The mTOR pathway is critical in epithelial regeneration in response to colitis (10, 11), and mTORC1 inactivation promotes colitis-induced CRC (12).

Regnase-1, also known as ZC3H12A and MCPIP1, is a CCCH-type zinc-finger protein (13, 14). Regnase-1 harbors a ribonuclease domain in its central region and negatively regulates the immune response through Toll-like receptors (TLRs) and IL-1 receptors by degradation of target mRNAs, such as IL-6 and the p40 subunit of IL-12 (15–18). Regnase-1 deficiency in mice causes severe autoimmune disease, leading to hyperactivation of T cells. In nonimmune cells, Regnase-1 maintains iron homeostasis in the duodenal epithelium (19). However, the role of Regnase-1 in the colon is not characterized. In this study, we examined the role of Regnase-1 in dextran sulfate sodium (DSS)-induced intestinal epithelial injury. We report that Regnase-1 controls regeneration of the colon epithelium by regulating mTOR and purine metabolism.

Results and Discussion

IEC-Specific Deletion of Regnase-1 in Mice. Regnase-1 is expressed in immune cells and in the large intestine (*SI Appendix*, Fig. S1*A*). To determine the function of Regnase-1 in the intestinal epithelium, we generated mice lacking Regnase-1 within the intestinal epithelium (hereafter termed Regnase-1$^{\Delta IEC}$) by breeding Regnase-1$^{fl/fl}$ mice with transgenic mice expressing intestine-specific Villin-Cre (20). The absence of *Regnase-1* mRNA in the colon and rectum was confirmed by RT-qPCR (*SI Appendix*, Fig. S1*B*). Regnase-1$^{\Delta IEC}$ mice are healthy and indistinguishable from control (Regnase-1$^{fl/fl}$) mice. Also, Regnase-1$^{\Delta IEC}$ mice show no symptoms of autoimmune disease, which is different from either the conventional or CD4-specific *Regnase-1*–deficient mice (15, 17). The length of the colon was significantly longer (*SI Appendix*, Fig. S1*C*) and the intestinal epithelial layer was thicker (*SI Appendix*, Fig. S1*D*) in Regnase-1$^{\Delta IEC}$ mice compared with control mice housed in the

Significance

Idiopathic inflammatory bowel disease (IBD) is associated with the gut microbiota and immune system of the host; however, the precise pathogenesis of IBD is poorly defined. We show that specific deletion of the endoribonuclease Regnase-1 in intestinal epithelial cells relieves the symptoms of experimental colitis during acute inflammation. Regnase-1 deficiency potentiates mTOR signaling and purine metabolism in the colon epithelium. These data provide insight into the role of epithelial Regnase-1 in IBD.

Author contributions: K.M. and S.A. designed research; Y.N., M.S., G.M., S.K.S., Y.K., X.S., and K.M. performed research; D.M., S.N., H.T., and T.S. contributed new reagents/analytic tools; D.M. and S.N. analyzed the metagenome; H.T. and T.S. provided the mutant mice; Y.N., M.S., G.M., K.M., and S.A. analyzed data; and K.M. wrote the paper.

Reviewers: K.H., Keio University; and M.N., Johannes Gutenberg University.

Conflict of interest statement: S.A. has research support from Chugai Pharmaceutical Co., Ltd. The terms of this arrangement have been reviewed and approved by Osaka University in accordance with its policy on objectivity in research. K.M. has a research collaboration with Otsuka Pharmaceutical Co., Ltd.

[1]Y.N., M.S., and G.M. contributed equally to this work.

[2]To whom correspondence should be addressed. Email: sakira@biken.osaka-u.ac.jp.

This article contains supporting information online at www.pnas.org/lookup/suppl/doi:10.1073/pnas.1809575115/-/DCSupplemental.

Published online October 8, 2018.

specific-pathogen-free facility. Immunohistochemistry showed increased numbers of Muc2+ and Alcian blue+ cells (*SI Appendix*, Fig. S1*D*), which also express the goblet cell marker *Gob5* (encoded by *Clca3*) (*SI Appendix*, Fig. S1*D*), indicating that Regnase-1$^{\Delta IEC}$ mice have increased numbers of goblet cells. FACS analysis of peripheral blood and spleen cells from Regnase-1$^{\Delta IEC}$ mice showed similar numbers of monocytes, neutrophils, and macrophages (*SI Appendix*, Fig. S2 *A* and *B*); therefore, the development of immune cells was normal. We also examined bacterial 16S ribosomal RNA genes to characterize the fecal microbial profiles from control and Regnase-1$^{\Delta IEC}$ mice. There was no significant difference in composition of the bacterial community at any taxonomic level (*SI Appendix*, Fig. S3). Taken together, these data indicate that the increase in the number of goblet cells in the intestinal epithelium in the absence of Regnase-1 is caused by an intrinsic mechanism.

Regnase-1$^{\Delta IEC}$ Mice Are Resistant to Experimental Colitis. To investigate the function of Regnase-1 in intestinal inflammation, DSS was administered in drinking water for 7 d to induce colitis (Fig. 1*A*). Control mice showed greater weight loss than Regnase-1$^{\Delta IEC}$ mice. Regnase-1$^{\Delta IEC}$ mice were resistant to the loss of body weight irrespective of sex (*SI Appendix*, Fig. S4*A*), even at a higher DSS dose (*SI Appendix*, Fig. S4*B*), indicating that Regnase-1 is involved in DSS-induced colitis. Regnase-1$^{AA/AA}$ mutant mice, which harbor the mutations of the IκB kinase phosphorylation sites, resulting in a degradation-resistant Regnase-1, exhibited the opposite effect (Fig. 1*B*), indicating that Regnase-1 is highly involved in IBD. The colon length at 9 d (after recovery with normal drinking water for 2 d) in Regnase-1$^{\Delta IEC}$ mice was significantly longer than that of controls (Fig. 1*C*). We evaluated the colon morphological architecture with H&E staining (Fig. 1*D* and *SI Appendix*, Fig. S5). Regnase-1$^{\Delta IEC}$ mice displayed fewer epithelial erosions, crypt damage, and infiltrating inflammatory cells in the colonic mucosa. The pathological score also shows the attenuation of inflammation in DSS-administrated Regnase-1$^{\Delta IEC}$ mice (Fig. 1*E*).

Alcian blue staining was consistent with Muc2 staining, indicating increased mucin production in Regnase-1$^{\Delta IEC}$ mice (Fig. 1*F*). To examine the target specificity of Regnase-1 by its ribonuclease activity, we cloned the 3′-UTRs of intestinal cell marker genes for enteroendocrine cells, goblet cells, and Tuft

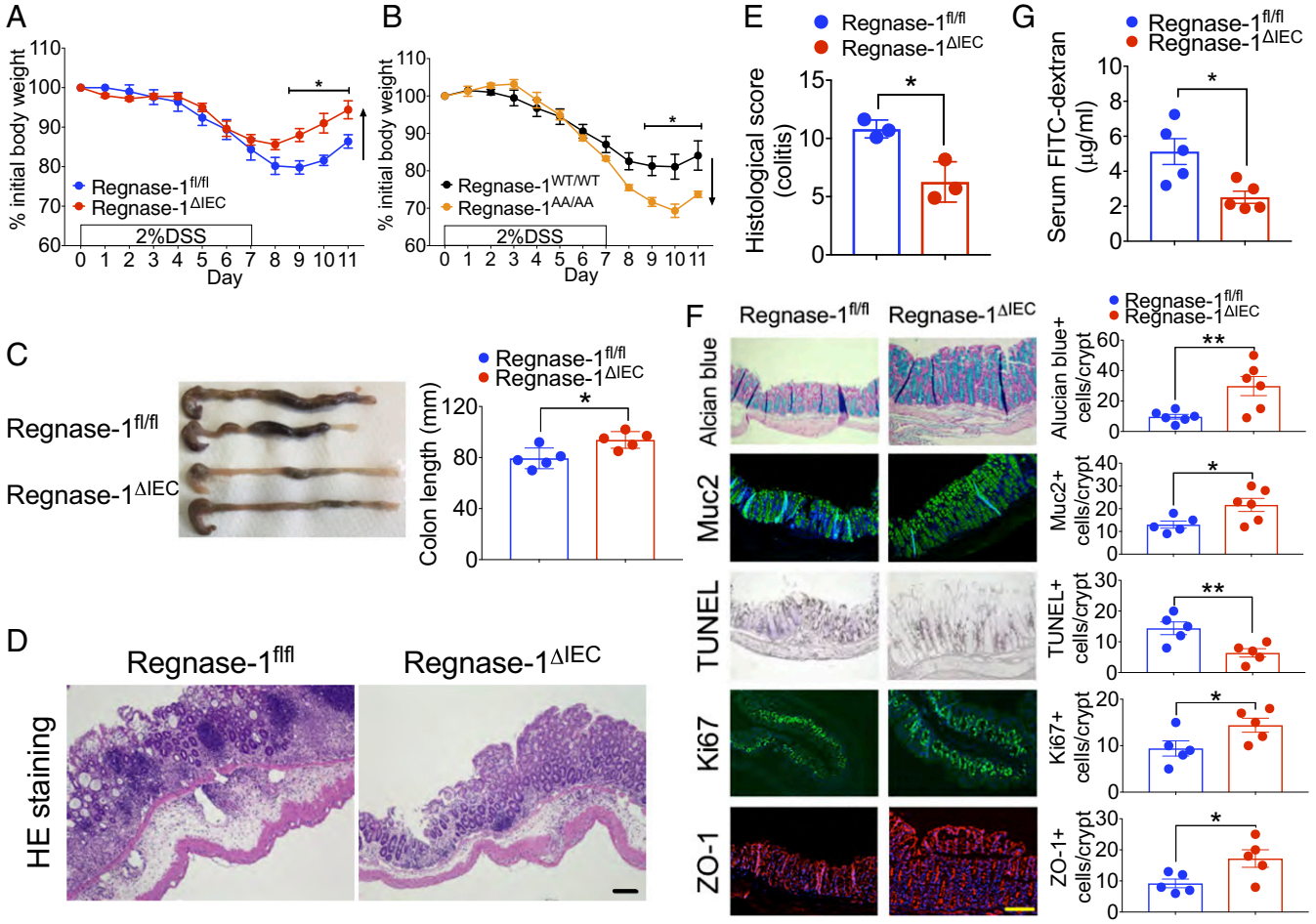

Fig. 1. Regnase-1$^{\Delta IEC}$ mice are resistant to experimental colitis. (*A*) Percentage change in 2% DSS-treated body weight compared with starting weight in Regnase-1$^{fl/fl}$ and Regnase-1$^{\Delta IEC}$ mice. (*B*) Percentage change in 2% DSS-treated body weight compared with starting weight in Regnase-1$^{WT/WT}$ and Regnase-1$^{AA/AA}$ mice. (*C*) Representative pictures of colons and colon length for Regnase-1$^{fl/fl}$ and Regnase-1$^{\Delta IEC}$ mice after DSS administration. (*D*) Representative DSS-treated colon sections from Regnase-1$^{fl/fl}$ and Regnase-1$^{\Delta IEC}$ mice stained with H&E. (*E*) Histological scoring for colitis. (*F*) Representative DSS-treated colon sections from Regnase-1$^{fl/fl}$ and Regnase-1$^{\Delta IEC}$ mice stained with Alcian blue, Muc2, TUNEL, Ki67, and ZO-1. (*Right*) Mean positive staining of cells counted in five crypts ($n = 5$). (*G*) FITC–dextran permeability assay. Plasma FITC–dextran concentrations following oral gavage (250 mg/kg body weight) in Regnase-1$^{fl/fl}$ and Regnase-1$^{\Delta IEC}$ mice are shown. Representative data from three (*A*, *C*, and *F*) and two (*B* and *G*) independent animal experiments (three to six mice per group) are shown. (Scale bars: 100 μm.) $^{*}P < 0.05$ and $^{**}P < 0.01$.

cells and performed luciferase assays (*SI Appendix*, Fig. S6). However, there was a nonspecific target gene among them, suggesting that the mucin production is a secondary effect of Regnase-1 deficiency. Decreased numbers of TUNEL-positive cells and increased numbers of Ki67-positive cells were also observed (Fig. 1*F*). These data suggest that Regnase-1 deficiency may facilitate normal healing to prevent the death and to enhance the proliferation of intestinal epithelial cells during colonic inflammation. The FITC–dextran absorption assay showed that the epithelial barrier was protected in Regnase-1$^{\Delta IEC}$ mice (Fig. 1*G*), consistent with less disruption of the tight junction protein ZO-1 (Fig. 1*F*). Taken together, these results show that the loss of Regnase-1 in the intestinal epithelium renders mice impervious to DSS-induced colitis.

Regnase-1 Targets to mTOR Signaling Pathway Associated with Colitis and Cancer. The combination of DSS and the carcinogen azoxymethane (AOM) induces colitis-associated CRC in mice (Fig. 2*A*). We examined whether Regnase-1 is associated with CRC. On day 65 of the protocol, each AOM/DSS-induced mouse harbored multiple colon tumors (Fig. 2*B*). Interestingly, reduced histological scores for colitis and tumor progression were observed in Regnase-1$^{\Delta IEC}$ mice (Fig. 2*C* and *SI Appendix*, Fig. S7). The expression of Reganse-1 was increased in both the acute and the chronic phase (Fig. 2*D*). These results indicate that Regnase-1 deficiency alleviated not only colitis but also colitis-induced CRC.

Intestinal regeneration is associated with the mTOR-signaling pathway (21), while mTORC1 signaling plays a crucial role in the regulation of various cellular processes (22–24). Rapamycin has been used as an inhibitor for studying mTOR function and signaling (4). Systemic administration of rapamycin to IBD model mice inhibits intestinal regeneration accompanied by loss of body weight (10). Administration of rapamycin and DSS caused a similar effect on loss of body weight in both Regnase-1$^{\Delta IEC}$ and control mice (Fig. 2*E*), indicating that the DSS resistance of Regnase-1$^{\Delta IEC}$ mice is mediated by mTOR signaling. We assessed the expression levels of mTOR-signaling proteins by Western blotting (Fig. 2*F*). The phosphorylation of mTOR was elevated in IECs of Regnase-1$^{\Delta IEC}$ mice. The levels of downstream the proteins S6K and 4E-BP1 were also increased (Fig.

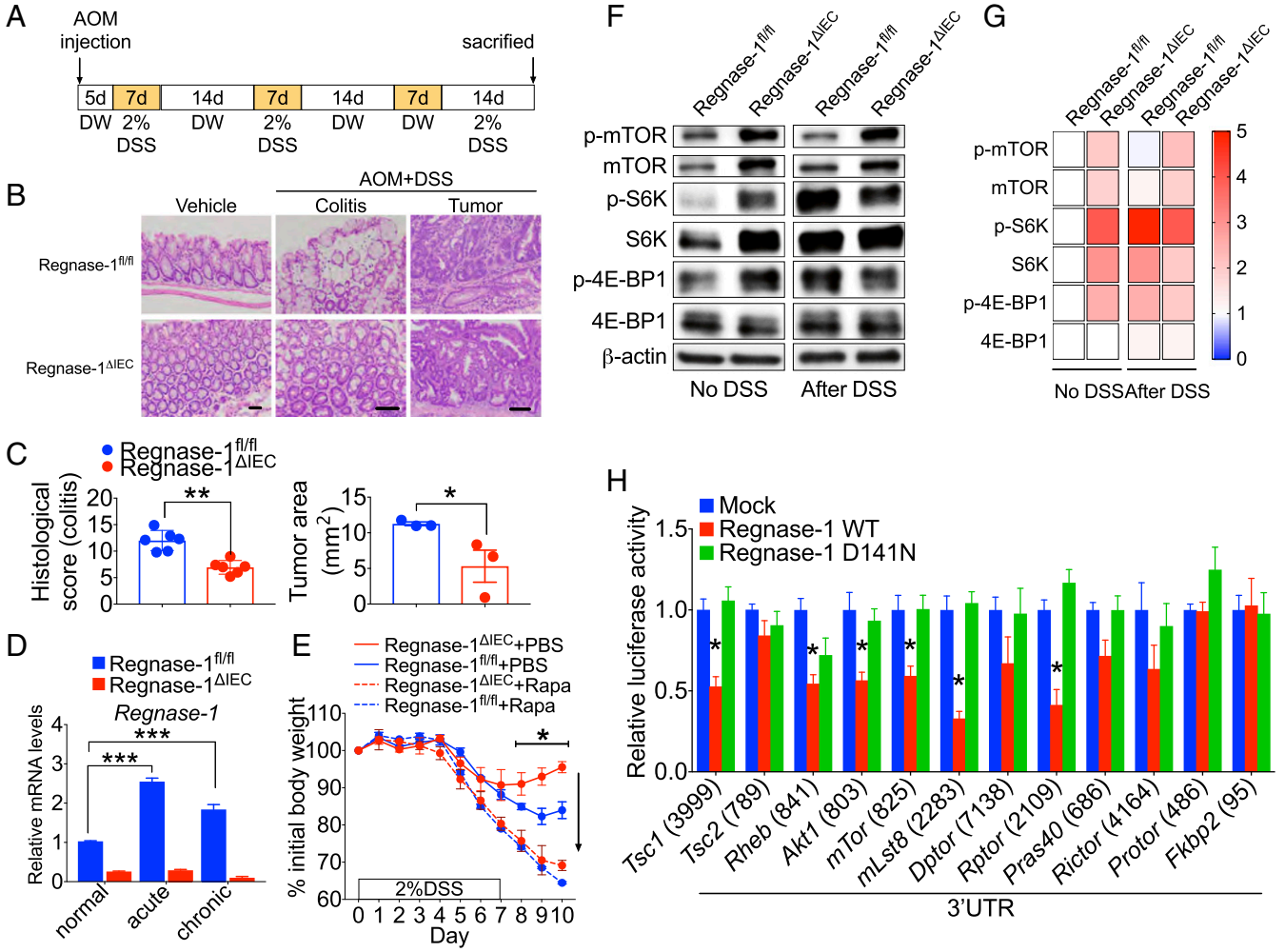

Fig. 2. Regnase-1 targets to mTOR-signaling pathway. (*A*) Protocol for AOM/DSS-treated colorectal cancer. (*B*) Representative colon tumor and colitis sections from Regnase-1$^{fl/fl}$ and Regnase-1$^{\Delta IEC}$ mice stained with H&E. (Scale bars: 50 μm.) (*C*) Histological scoring for colitis and tumors. Tumor nodules of Regnase-1$^{fl/fl}$ and Regnase-1$^{\Delta IEC}$ mice were compared. (*D*) Expression levels of Regnase-1 in acute and chronic phase of DSS-induced colitis. (*E*) Percentage change in 2% DSS-treated body weight compared with starting weight in Regnase-1$^{fl/fl}$ and Regnase-1$^{\Delta IEC}$ mice and rapamycin (10 mg/kg body weight) plus DSS-treated mice. (*F*) Western blot analysis of mTOR-signaling-pathway proteins from Regnase-1$^{fl/fl}$ and Regnase-1$^{\Delta IEC}$ mice with or without DSS treatment. (*G*) Relative amounts of indicated protein are shown in heat map. Protein amount of Regnase-1$^{fl/fl}$ without DSS treatment was set as onefold. (*H*) Luciferase assays for 3′-UTRs of mTOR-signaling-pathway proteins. The length of each 3′-UTR is indicated in parentheses. Representative data from two independent animal experiments (three to six mice per group) (*A*–*G*) and three independent experiments (*H*) are shown. $*P < 0.05$, $**P < 0.01$, and $***P < 0.001$.

2*G*). The increased level of mTOR was maintained even after DSS treatment (Fig. 2*G*), indicating that mTOR signaling is constitutively activated in IECs of Regnase-1$^{\Delta IEC}$ mice. By 3′-UTR luciferase assays for mTOR-signaling proteins, Regnase-1 significantly reduced the luciferase activity of *Tsc1*, *Rheb*, *Akt1*, *mTor*, *mLst8*, and *Rptor*, which are the main components of mTORC1 (Fig. 2*H*), indicating that Regnase-1 controls the mTORC1 pathway more than the mTORC2 (*SI Appendix*, Fig. S8).

Regnase-1 Is Involved in the Purine Metabolic Pathway. Both initiation and resolution of inflammation are accompanied by metabolic reprogramming. To investigate whether Regnase-1 regulates IEC metabolism, we performed a metabolome analysis. We detected altered levels of purine metabolites in Regnase-1$^{\Delta IEC}$ mice. The production of intracellular ATP was markedly increased in freshly isolated IECs from Regnase-1$^{\Delta IEC}$ mice (Fig. 3*A*). In contrast, the amounts of ADP and AMP were decreased. The level of adenosine was also markedly reduced, while levels of inosinic acid and its degradation products were elevated (Fig. 3 *A* and *B*).

Several enzymes are involved in this purine metabolism pathway. Xanthine oxidase (Xod, also known as xanthine dehydrogenase) converts hypoxanthine to xanthine and then to uric acid. Adenosine deaminase (Ada) catalyzes adenosine to inosine. Adenylate kinase-1 (Ak1) catalyzes AMP/ADP to ATP (Fig. 3*B*). To assess the effect of these enzymes in vivo, we used two inhibitors, an Ada inhibitor [erythro-2-(2-hydroxy-3-nonyl)adenine (EHNA)] and a Xod inhibitor (Allopurinol), with the DSS IBD model. EHNA administration caused significant loss of body weight in Regnase-1$^{\Delta IEC}$ and control mice (Fig. 3*C*, *Left*), indicating that Ada-mediated enzyme activity was elevated in Regnase-1$^{\Delta IEC}$ mice. This result also indicates that EHNA administration may elevate the concentration of adenosine and converted AMP, leading to activation of AMP-activated protein kinase and attenuation of mTOR signaling. Allopurinol also caused body weight loss in Regnase-1$^{\Delta IEC}$ mice (Fig. 3*C*, *Right*), indicating that blocking uric acid production may enhance intestinal damage during inflammation in Regnase-1$^{\Delta IEC}$ mice. Conversely, inosine administration attenuated colitis, as reported previously (*SI Appendix*, Fig. S9) (25). This increased level of inosine may enhance the endogenous antioxidant system. Antiinflammatory effects of inosine are mediated by the activation of adenosine receptors that protect against the development of disease in several murine disease models (26, 27). mTOR is essential for Xod activation (28); therefore, Regnase-1 regulates purine catabolism by up-regulating mTOR. Next, we examined target specificity using luciferase assays. Regnase-1 significantly reduced the luciferase activity of *Ak1* and *Xod* but not of *Ada* (Fig. 3*D*), indicating that Regnase-1 targets these genes. These results reveal that Regnase-1 deficiency in IECs promotes purine anabolism and catabolism.

Metabolome analysis during DSS administration identified increases in uric acid, xanthine, and hypoxanthine in IECs of Regnase-1$^{\Delta IEC}$ mice (Fig. 3*E*), indicating that Regnase-1 negatively regulates the purine catabolic pathway. Also during the first 7 d of DSS-injury induction, basal oxygen consumption rate and the extracellular acidification rate were gradually altered (Fig. 3*F*). The ablation of Regnase-1 seems to prevent down-regulation

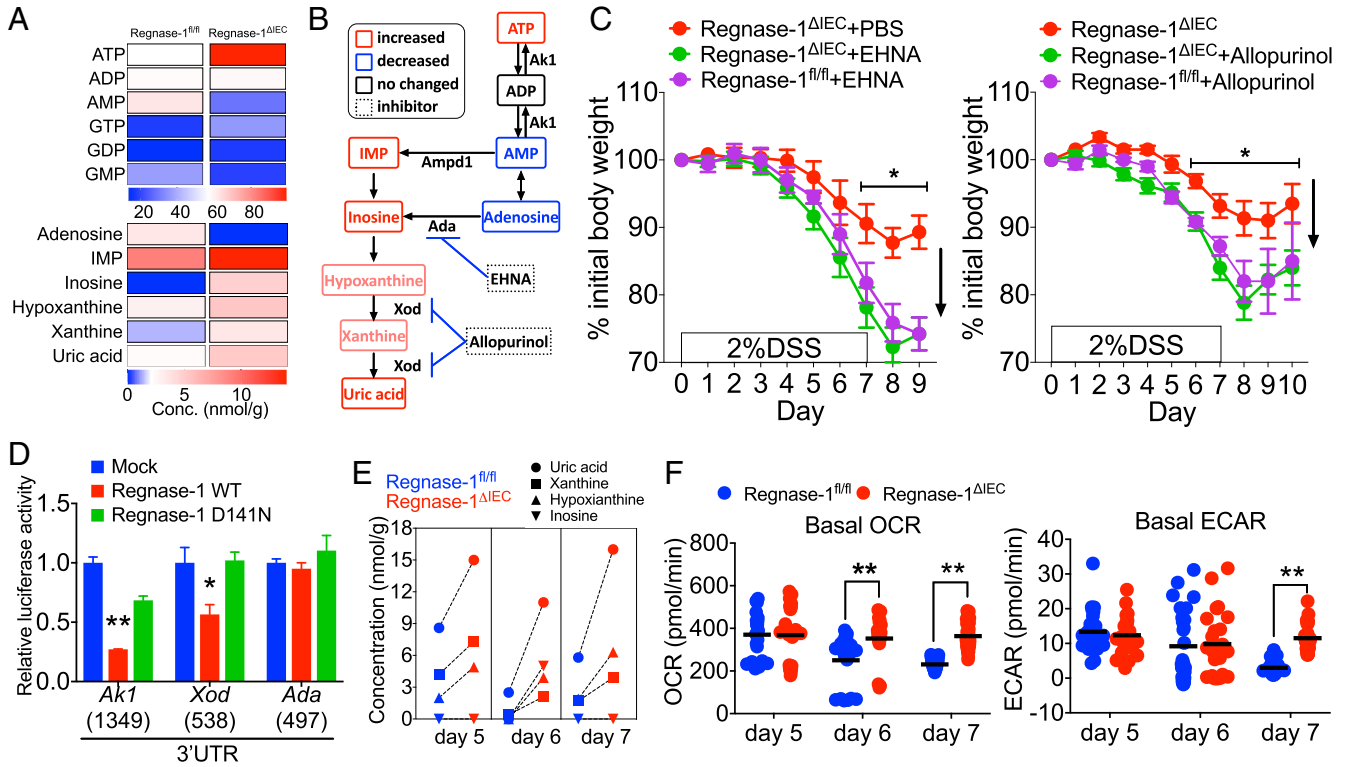

Fig. 3. Regnase-1 is involved in the purine metabolic pathway. (*A*) Analysis of the metabolites in normal IECs from Regnase-1$^{fl/fl}$ and Regnase-1$^{\Delta IEC}$ mice. (*B*) Purine metabolic pathway. Increased and decreased levels of metabolites from IECs of Regnase-1$^{\Delta IEC}$ mice are indicated by red and blue, respectively. Unchanged metabolites and enzyme inhibitors are indicated by black and dot-lined boxes, respectively. (*C*) Percentage change in 2% DSS-treated body weight compared with starting weight of Regnase-1$^{\Delta IEC}$ mice administered PBS or EHNA (0.3 mg/kg, i.p.) (*Left*) and with or without Allopurinol (1 mg/mL) in drinking water (*Right*). (*D*) Luciferase assay for the 3′-UTRs of *adenosine kinase 1* (*Ak1*), *xanthine oxidase* (*Xod*), and *adenosine deaminase* (*Ada*). The length of each 3′-UTR is indicated in parentheses. (*E*) Major changes to purine metabolites in IECs during DSS administration. (*F*) Seahorse analysis of basal oxygen consumption rate (*Left*) and basal extracellular acidification rate (*Right*) in IECs from DSS-treated mice. Data from one experiment (*A*, *B*, and *E*: cells pooled from four to six mice per time point) and representative data from two independent experiments (five mice per group) (*C*) and three independent experiments (*D* and *F*) are shown. $*P < 0.05$ and $**P < 0.01$.

of the metabolic state in response to inflammation. Of note, the mitochondrial respiration bioenergetics parameters, ATP-linked respiration, proton leak, and maximal and reserve capacity were higher in IECs of Regnase-1$^{\Delta IEC}$ mice at day 7 (*SI Appendix*, Fig. S10*A*), indicating that Regnase-1 negatively regulates regeneration after inflammation by modulating energy metabolism. Consistent with this, the weight of crypts was significantly elevated in Regnase-1$^{\Delta IEC}$ mice until day 7 during DSS-injury induction (*SI Appendix*, Fig. S10*B*). Hypoxia is also an important factor in the inflammatory microenvironment that affects adenosine and hypoxia-inducible factor signaling (29). Profound hypoxia is associated with IBD; however, the expression of both *Hif1a* and *Epas1* (Hif2a) mRNA was not different between control and knockout mice (*SI Appendix*, Fig. S11). Collectively, these data demonstrate that purine metabolism is consistently increased in IECs of Regnase-1$^{\Delta IEC}$ mice.

Regulation of Ectonucleotidases by Regnase-1. CD73 (encoded by *Nt5e*) and CD39 (*Entpd1*) are extracellular receptors of the ATP catalyzing pathway (Fig. 4*A*). Both transcripts were elevated in IECs of Regnase-1$^{\Delta IEC}$ mice (Fig. 4*B*). The expression of *Cd73* in IECs of Regnase-1$^{\Delta IEC}$ mice was consistently higher compared with that in control mice (Fig. 4*B*). The expression of *Cd39* in IECs of Regnase-1$^{\Delta IEC}$ mice gradually decreased compared with that in control mice during the course of DSS administration (Fig. 4*B*). *Cd39* and *Cd73* knockout mice have severe colitis; therefore, the expression of both is protective against DSS-induced colitis due to the depletion of proinflammatory ATP signaling (30, 31). These ectonucleotidases shift ATP-driven proinflammatory immune cell activity toward an antiinflammatory state mediated by adenosine (32). Increased numbers of extracellular receptors on IECs of Regnase-1$^{\Delta IEC}$ mice may contribute to resolution of the inflammation.

Extracellular adenosine interacts with P1 purinergic receptors (Fig. 4*A*). Among them, expression of the adenosine A1 receptor (A1R, encoded by *Adora1*), which has the highest affinity for adenosine, was significantly increased in Regnase-1$^{\Delta IEC}$ mice after DSS-induced colitis at days 5 and 7 (Fig. 4*C*), but levels of other receptors—A2AR (*Adora2a*), A2BR (*Adora2b*), and A3R (*Adora3*), as well as the equilibrative nucleoside transporters ENTs, Ent1 (*Slc29a1*), and Ent2 (*Slc29a2*)— were not markedly changed (Fig. 4*C*). Notably, the expression of Regnase-1 in the control mice was elevated during DSS injury, as well as under chronic inflammatory conditions (Figs. 4*C* and 2*D*). This suggests the potential relevance of Regnase-1 as a promising target structure in IBD or CRC for therapeutic intervention.

We performed luciferase assays for the full-length and deleted 3′-UTRs of *Cd73*, *Cd39*, and *Adora1* genes (Fig. 4*D* and *SI Appendix*, Fig. S12). The luciferase activity was significantly reduced by wild-type Regnase-1, indicating that these genes are targeted by Regnase-1. An increased level of A1R may cooperate with CD73 to maintain epithelial barrier integrity and inhibition of inflammation to prevent tumor progression (33). Taken together, these data show that Regnase-1 deficiency reduces inflammation by up-regulating expression of ectonucleotidases.

We demonstrated in vivo the relevance of Regnase-1 in colitis. Regnase-1$^{\Delta IEC}$ mice are resistant to DSS-induced colitis, leading to increased proliferation and reduced apoptosis of IECs. In conclusion, we found that Regnase-1 controls regeneration of the colon epithelium by regulating mTOR and purine metabolism.

Materials and Methods

Mice. Regnase-1$^{fl/fl}$ and Villin-Cre mice have been described previously (17, 20). Regnase-1$^{AA/AA}$ mutant mice were generated by homologous recombination. All mice were housed under specific-pathogen-free conditions. All animal experiments were performed with approval of the Animal Research Committee of the Research Institute for Microbial Diseases, Osaka University.

DSS-Induced Colitis. Eight- to 12-wk-old Regnase-1$^{fl/fl}$ and Regnase-1$^{\Delta IEC}$ mice and 20-wk-old Regnase-1$^{WT/WT}$ and Regnase-1$^{AA/AA}$ mice were used for DSS-induced colitis experiments. Acute colitis was induced by administration of drinking water containing 2 or 3% DSS (36–50 kDa; MP Biomedicals) for 7 d, which was changed to normal water for an additional 2–3 d. Chronic colitis was induced by three cycles of 2% DSS (7 d of DSS induction, 14 d of water). Mice were analyzed for body weight and/or histological changes. Rapamycin (10 mg/kg body weight; Sigma), EHNA (0.3 mg/kg of body weight; Sigma), and PBS were intraperitoneally injected into mice every day during DSS administration. Allopurinol (1 mg/mL; Nichi-Iko Pharmaceutical) was administered by supplementation of drinking water during DSS administration.

Immunohistochemistry, Immunofluorescence, and TUNEL Analysis. Freshly isolated colon was fixed in formaldehyde and embedded in paraffin. Immunohistochemical staining was performed using the DAKO Envision System for primary antibodies according to the manufacturer's protocol. TUNEL staining was performed using an in situ Apoptosis Detection Kit (Takara). H&E staining was performed using a standard protocol. Images were captured using a BZ-9000 microscope (Keyence). The antibodies used are described in *SI Appendix*.

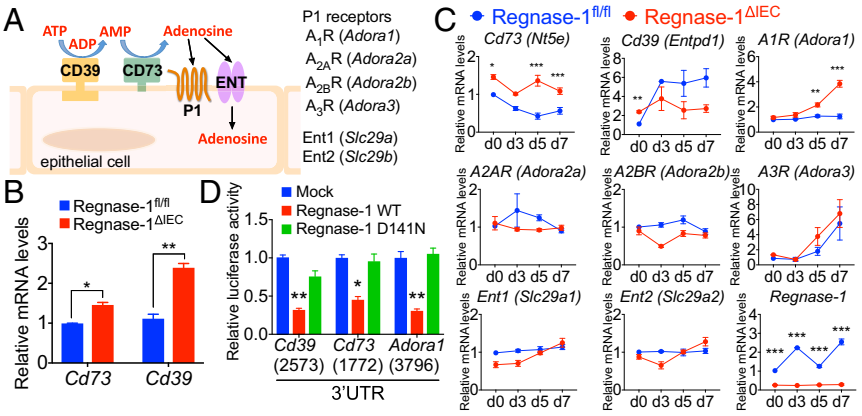

Fig. 4. Regulation of ectonucleotidases by Regnase-1. (*A*) Cartoon of the ATP transport pathway. (*B*) Levels of *Cd73* and *Cd39* mRNAs in normal IECs from Regnase-1$^{fl/fl}$ and Regnase-1$^{\Delta IEC}$ mice. (*C*) Analysis of gene expression of ATP receptors and Regnase-1 in IECs during DSS administration. Expression of Regnase-1$^{fl/fl}$ in day 0 was set as 1. (*D*) Luciferase assays for 3′-UTRs of *Cd39*, *Cd73*, and *Adora1*. The length of each 3′-UTR is indicated in parentheses. Representative data from two independent animal experiments (three to five mice per group) (*B* and *C*) and three independent experiments (*D*) are shown. $*P < 0.05$, $**P < 0.01$, and $***P < 0.001$.

Histological Scoring. Scoring of colonic inflammation was determined as described by Rath et al. (34) with slight modifications and assessed goblet cells, mucosa thickening, inflammatory cells, and submucosa cell infiltration. Each criterion was scored as 0–4, and the sum of each score was defined as the histological score.

FITC–Dextran Permeability Assay. Intestinal permeability was assessed by luminal enteral administration of FITC–dextran 4000 (Sigma). Mice were given FITC–dextran (250 mg/kg body weight) by oral gavage 4 h before drawing blood. The amount of FITC–dextran in plasma was measured in duplicate using a fluorometer (ARVO, Perkin-Elmer). Dilutions of FITC–dextran in PBS were used to generate a standard curve, and absorption of 25 μL of plasma or standard was measured in a fluorometer at 488 nm.

Isolation of Crypts. Large intestine tissue fragments were incubated with 5 mM EDTA and 1 mM DTT in PBS for 30 min on ice. After removal of EDTA, repeated vigorous shaking of the sample with cold PBS and centrifugation yielded pellets enriched in villi and crypts.

Western Blot Analysis. Isolated crypts from the large intestine were homogenized in RIPA buffer. Western blot signals were analyzed by densitometric measurements and subsequently quantified using the National Institutes of Health Image software program. Used antibodies are provided in *SI Appendix*.

Metabolomic Analysis. To measure the metabolites of IECs, isolated IECs from four mice were pooled for each independent measurement. Extracts (>20 mg) were prepared from 10^6 cells with methanol containing internal standard solution (Human Metabolome Technologies). Cationic compounds were measured in the positive mode of capillary electrophoresis–connected time-of-flight mass spectrometry, and anionic compounds were measured in the positive and negative modes of capillary electrophoresis–tandem mass spectrometry.

Assessment of Bioenergetics. Isolated IECs from 500 crypts were plated with Matrigel in culture media on Seahorse Extracellular Analyzer XFp (Agilent-Seahorse XF Technology) plates. Oxygen consumption rate and extracellular acidification rate were measured on a Seahorse XFp analyzer (Agilent) in the presence of the mitochondrial complex V inhibitor oligomycin (5 μM), mitochondrial uncoupler FCCP (5 μM), and respiratory chain inhibitor antimycin A/rotenone (0.1 μM).

Quantitative PCR Analysis. Total RNA from the EpCAM+CD45− population was isolated with an RNeasy plus mini kit (Qiagen), and reverse transcription was performed with SuperScript III (Thermo Fishers Scientific). For quantitative PCR, cDNA fragments were amplified using a Thunderbird Probe One-step qRT-PCR Kit (Toyobo). TaqMan probes for murine genes of interest were purchased from Applied Biosystems. Fluorescence was detected with a ViiA-7 Real-Time PCR system (Applied Biosystems). mRNA levels were normalized to those of 18S rRNA. Primer sequences are listed in *SI Appendix*.

Luciferase Assay. HEK293 cells were transfected with pGL3-3′-UTR for the mRNAs of interest or pGL3-empty plasmid together with a wild-type or nuclease-defective (D141N) Regnase-1 expression plasmid or empty control plasmid. After 2 d of culture, cells were lysed, and luciferase activities in the lysates were determined using the dual-luciferase reporter assay system (Promega). The *Renilla* luciferase expression vector was simultaneously transfected as an internal control. Primer sequences used to isolate each 3′-UTR are provided in *SI Appendix*.

Statistical Analysis. Statistical analysis of experimental data was performed using GraphPad Prism version 7. All P values <0.05 were considered significant. Error bars denote the SEM.

ACKNOWLEDGMENTS. We thank K. Asakawa and M. Tasai for technical assistance; E. Kamada for secretarial assistance; and Dr. K. Takeda (Osaka University) and Dr. M. J. Caldez for critical reading of the manuscript. This work was supported in part by Grant-in-Aid for Specially Promoted Research Grant 15H05704 (to S.A.) and by Scientific Research (C) Grant 18K07173 (to K.M.) of the Japan Society for the Promotion of Science.

1. Sun L, Nava GM, Stappenbeck TS (2011) Host genetic susceptibility, dysbiosis, and viral triggers in inflammatory bowel disease. *Curr Opin Gastroenterol* 27:321–327.
2. Brenner H, Kloor M, Pox CP (2014) Colorectal cancer. *Lancet* 383:1490–1502.
3. Kiesler P, Fuss IJ, Strober W (2015) Experimental models of inflammatory bowel diseases. *Cell Mol Gastroenterol Hepatol* 1:154–170.
4. Laplante M, Sabatini DM (2012) mTOR signaling in growth control and disease. *Cell* 149:274–293.
5. Xu K, Liu P, Wei W (2014) mTOR signaling in tumorigenesis. *Biochim Biophys Acta* 1846:638–654.
6. Robitaille AM, et al. (2013) Quantitative phosphoproteomics reveal mTORC1 activates de novo pyrimidine synthesis. *Science* 339:1320–1323.
7. Ben-Sahra I, Howell JJ, Asara JM, Manning BD (2013) Stimulation of de novo pyrimidine synthesis by growth signaling through mTOR and S6K1. *Science* 339:1323–1328.
8. Ben-Sahra I, Hoxhaj G, Ricoult SJH, Asara JM, Manning BD (2016) mTORC1 induces purine synthesis through control of the mitochondrial tetrahydrofolate cycle. *Science* 351:728–733.
9. Malley CO, Pidgeon GP (2015) The mTOR pathway in obesity driven gastrointestinal cancers: Potential targets and clinical trials. *BBA Clin* 5:29–40.
10. Guan Y, et al. (2015) Repression of mammalian target of rapamycin complex 1 inhibits intestinal regeneration in acute inflammatory bowel disease models. *J Immunol* 195: 339–346.
11. Sampson LL, Davis AK, Grogg MW, Zheng Y (2016) mTOR disruption causes intestinal epithelial cell defects and intestinal atrophy postinjury in mice. *FASEB J* 30:1263–1275.
12. Brandt M, et al. (2018) mTORC1 inactivation promotes colitis-induced colorectal cancer but protects from APC loss-dependent tumorigenesis. *Cell Metab* 27: 118–135.e8.
13. Fu M, Blackshear PJ (2017) RNA-binding proteins in immune regulation: A focus on CCCH zinc finger proteins. *Nat Rev Immunol* 17:130–143.
14. Maeda K, Akira S (2017) Regulation of mRNA stability by CCCH-type zinc-finger proteins in immune cells. *Int Immunol* 29:149–155.
15. Matsushita K, et al. (2009) Zc3h12a is an RNase essential for controlling immune responses by regulating mRNA decay. *Nature* 458:1185–1190.
16. Iwasaki H, et al. (2011) The IκB kinase complex regulates the stability of cytokine-encoding mRNA induced by TLR-IL-1R by controlling degradation of regnase-1. *Nat Immunol* 12:1167–1175.
17. Uehata T, et al. (2013) Malt1-induced cleavage of regnase-1 in CD4(+) helper T cells regulates immune activation. *Cell* 153:1036–1049.
18. Mino T, et al. (2015) Regnase-1 and roquin regulate a common element in inflammatory mRNAs by spatiotemporally distinct mechanisms. *Cell* 161:1058–1073.
19. Yoshinaga M, et al. (2017) Regnase-1 maintains iron homeostasis via the degradation of transferrin receptor 1 and prolyl-hydroxylase-domain-containing protein 3 mRNAs. *Cell Rep* 19:1614–1630.
20. el Marjou F, et al. (2004) Tissue-specific and inducible Cre-mediated recombination in the gut epithelium. *Genesis* 39:186–193.
21. Yang J, et al. (2015) Rapamycin inhibition of mTOR reduces levels of the Na+/H+ exchanger 3 in intestines of mice and humans, leading to diarrhea. *Gastroenterology* 149:151–162.
22. Bar-Peled L, Sabatini DM (2014) Regulation of mTORC1 by amino acids. *Trends Cell Biol* 24:400–406.
23. Djouder N, et al. (2007) S6K1-mediated disassembly of mitochondrial URI/PP1gamma complexes activates a negative feedback program that counters S6K1 survival signaling. *Mol Cell* 28:28–40.
24. Dowling RJ, et al. (2010) mTORC1-mediated cell proliferation, but not cell growth, controlled by the 4E-BPs. *Science* 328:1172–1176.
25. Mabley JG, et al. (2003) Inosine reduces inflammation and improves survival in a murine model of colitis. *Am J Physiol Gastrointest Liver Physiol* 284:G138–G144.
26. Haskó G, et al. (2000) Inosine inhibits inflammatory cytokine production by a post-transcriptional mechanism and protects against endotoxin-induced shock. *J Immunol* 164:1013–1019.
27. Haskó G, Sitkovsky MV, Szabó C (2004) Immunomodulatory and neuroprotective effects of inosine. *Trends Pharmacol Sci* 25:152–157.
28. Abooali M, et al. (2014) Crucial involvement of xanthine oxidase in the intracellular signalling networks associated with human myeloid cell function. *Sci Rep* 4:6307.
29. Colgan SP, Eltzschig HK (2012) Adenosine and hypoxia-inducible factor signaling in intestinal injury and recovery. *Annu Rev Physiol* 74:153–175.
30. Bynoe MS, et al. (2012) CD73 is critical for the resolution of murine colonic inflammation. *J Biomed Biotechnol* 2012:260983.
31. Friedman DJ, et al. (2009) From the cover: CD39 deletion exacerbates experimental murine colitis and human polymorphisms increase susceptibility to inflammatory bowel disease. *Proc Natl Acad Sci USA* 106:16788–16793.
32. Antonioli L, Pacher P, Vizi ES, Haskó G (2013) CD39 and CD73 in immunity and inflammation. *Trends Mol Med* 19:355–367.
33. Bowser JL, et al. (2016) Loss of CD73-mediated actin polymerization promotes endometrial tumor progression. *J Clin Invest* 126:220–238.
34. Rath HC, et al. (1996) Normal luminal bacteria, especially Bacteroides species, mediate chronic colitis, gastritis, and arthritis in HLA-B27/human beta2 microglobulin transgenic rats. *J Clin Invest* 98:945–953.